Inorganic Chemistry

Article

pubs.acs.org/IC

Heme Bound Amylin: Spectroscopic Characterization, Reactivity, and Relevance to Type 2 Diabetes

Soumya Mukherjee and Somdatta Ghosh Dey*

Department of Inorganic Chemistry, Indian Association for the Cultivation of Science, Jadavpur, Kolkata, India 700032

Supporting Information

ABSTRACT: Deposition of human amylin or islet amyloid polypeptide (hIAPP) within the β-cells of the pancreatic islet of Langerhans is implicated in the etiology of type 2 diabetes mellitus (T2Dm). Accumulating evidences suggest that increased body iron stores, iron overload, and, in particular, higher heme-iron intake is significantly associated with higher risk of Type 2 diabetes mellitus (T2Dm) (*PloS One* **2012**, *7*, e41641). Some key pathological features of T2Dm, like iron dyshomeostasis, iron accumulation, mitochondrial dysfunction, and oxidative stress are very similar to the cytopathologies of Alzheimer's disease, which have been invoked to be due to heme complexation with amyloid β peptides. The similar etiology and pathogenic features in both Alzheimer's disease (AD) and T2Dm indicate a common underlying mechanism, with heme playing an important role. In this study we show that hIAPP can bind heme. His18 residue of hIAPP binds heme under physiological conditions and results in an axial high-spin active site with a trans-axial water derived ligand. Arg11 is a key residue that is also essential for heme binding. Heme(Fe^{2+})-hIAPP complexes are prone to produce partially reduced oxygen species (PROS). The His18 residue identified in this study is absent in rats which do not show T2Dm, implicating the significance of this residue as well as heme in the pathology of T2Dm.

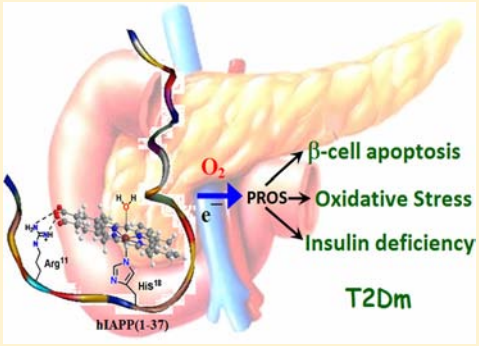

1. INTRODUCTION

Type 2 diabetes mellitus (T2Dm) is the most common chronic metabolic disorder characterized by dysfunction in both insulin action and insulin secretion from the β-cells of pancreatic islets of Langerhans, resulting in hyperglycemia.[1] Recent literature shows that protein aggregation, amyloidosis, and fibril formation are the central processes in many diseases like Alzheimer's disease (AD), Parkinson Disease, and T2Dm.[2−4] The invariant histopathological feature of patients suffering from T2Dm is the presence of fibrillar amyloid deposits in and around the β-cells of the pancreas.[1,4,5] The principal constituent of these amyloid deposits is a polypeptide hormone called amylin or Islet Amyloid Polypeptide Protein (IAPP) comprising of 37 amino-acid residues.[6,7] IAPP is coproduced and cosecreted with insulin by the pancreatic β-cells and have complementary hormonal activities.[8,9] Human IAPP (hIAPP) is a highly amyloidogenic peptide, with residues 20−29 forming the part of its amyloidogenic core.[10] Several reports indicate that aggregation of hIAPP(1−37) is responsible for the death of the pancreatic β-cells;[4,11,12] however, it is increasingly becoming apparent that it is the smaller oligomers that have the ability to induce membrane instability and β-cell apoptosis.[13−16] These soluble oligomers can induce oxidative stress by the spontaneous generation of PROS, for example, H_2O_2, and other free radicals.[17,18] The H_2O_2 generated is freely permeable across cell membranes and in the presence of reduced transition metal ions (Fe^{2+}, Cu^{+}) can generate cytotoxic hydroxyl radicals.[19]

Emerging scientific evidences have undisputedly established the potential link of body iron stores and iron influenced glucose metabolism in the etiopathogenesis of T2Dm.[20−22] Iron is a strong pro-oxidant and participates in the generation of reactive oxygen species such as hydroxyl radicals when present in excess and unshielded, resulting in the consequent elevation in oxidative stress.[23] Iron-induced oxidative stress on the β-cells along with iron deposition in the pancreatic β-cells results in their apoptosis which consequently leads to insulin deficiency.[24−26] Insulin resistance is also induced by iron deposition inhibiting glucose uptake in skeletal muscles and adipose tissues, with reduction in liver capacity to extract insulin, resulting in an abnormal hepatic glucose production.[27,28] Compared to other cell types, pancreatic β-cells are extremely susceptible to damage by partially reduced oxygen species (PROS),[17] probably because the islet cells almost exclusively rely on mitochondrial metabolism of glucose for glucose-induced insulin secretion and contain relatively very low levels of several PROS detoxifying systems.[25,29]

AD, the most common form of dementia in the elderly, is a neurodegenerative disorder.[30] AD is marked by the formation of senile plaques composed of aggregated amyloid beta (Aβ) peptides and the generation of PROS in the brain.[2,31] There is excessive accumulation of iron (especially heme *b*) in the brain of AD patients in the same region that are characterized by Aβ

Received: January 17, 2013
Published: April 23, 2013

   dx.doi.org/10.1021/ic4001413 | *Inorg. Chem.* 2013, 52, 5226−5235

deposition.[32] Such abnormal increase in the heme concentration in the brain of AD patients has been associated with the complexation of heme with Aβ peptides. The active site environment and enzymatic activity of the heme-Aβ complexes have been widely investigated to show that they behave as peroxidases, and the mechanism of generation of neurotoxic PROS has been elucidated.[32−34] This complexation leads to heme depletion and ultimately results in major symptoms like elevation in iron intake, increase of stress-related enzymes or proteins such as heme oxygenase-1 and transferrin, high bilirubin concentration,[35,36] abnormal iron homeostasis, decay of iron regulatory proteins, dysfunction of mitochondrial complex IV,[31,37] oxidative stress, and so forth. Incidentally the symptoms of AD are also common pathological features of T2Dm.[38,39] Given the overwhelming similarities between AD and T2Dm with respect to the involvement of iron and generation of oxidative stress, and the fact that evidence indicate that heme binding to Aβ peptides is a significant contributor for the pathology of AD, heme binding to hIAPP may lead to the cytopathologies of T2Dm resulting in the β-cell dysfunction.

Recent prospective cohort studies and systematic meta-analysis have positively associated high heme iron intake, the major dietary resource of body iron stores, with high risk of developing T2Dm.[40−42] Studies have also linked high heme iron intake with increased possibility of developing gestational diabetes.[43] Women diagnosed with gestational diabetes have a 22−60% chance of developing T2Dm in the future.[44,45] Thus, there could be a crucial involvement of heme in the T2Dm pathology, which would open up a new dimension in T2Dm research and may hold a key toward development of a cure. In this study we show that heme can bind hIAPP and investigate the active site environment of these complexes. The three well-known amino-acid residues present in hIAPP(1−37) are histidine (His18), cysteine (Cys2 and Cys7), and tyrosine (Try37) that are commonly involved in binding heme biologically. Arginine residue, though it does not bond directly with the heme-Fe, is often involved in secondary interactions near the active site, stabilizing it and enhancing the reactivity.[33,46] The hIAPP(1−37) has a single arginine residue (Arg11). Different spectroscopic techniques, absorption, resonance Raman (rR), and electron paramagnetic resonance (EPR), have been used to identify the amino acid residue of the hIAPP peptide that binds to heme, using native hIAPP(1−37) peptide, various isolated peptide fragments, and site directed mutants. CO binding to the reduced heme-hIAPP complexes provides insight into the nature of the active site environment, along with the elucidation of the key second sphere residue. We evaluated the effect of pH on these heme bound hIAPP peptide complexes to elucidate the nature of the exchangeable sixth ligand. Finally, we demonstrate and quantify that heme bound hIAPP can generate cytotoxic PROS.

2. EXPERIMENTAL METHODS

All reagents were of the highest grade commercially available and were used without further purification. Amylin (hIAPP) peptides of various amino-acid residues (1−37, 1−19, 1−22, and 20−37) have been used for this study. All site directed mutants are of hIAPP(1−19) peptide. The mutants used were His18Asn, His18Gly, Arg11Asn, and double mutant: Arg11Asn, His18Asn. All peptides were purchased from GL Biochem (Shanghai) Ltd. with >95% purity. Hemin, xylenol orange and buffers were purchased from Sigma, while sodium dithionite and Mohr's salt were purchased from Merck. Different buffers were used at different pHs: MES for pH (5−6.4), HEPES and phosphate for pH (7−9.5). All the peptide stock solutions for absorption spectra were made in 100 mM pH 7 phosphate buffer, hIAPP(1−37) peptide stock was made in 5 mM pH 5.5 Mes buffer. A stock of heme solution was made by dissolving hemin chloride in 1 M NaOH solution, and the concentration of the heme solution was determined spectrophotometrically (ε_{385} = 58.44 mM^{-1} cm^{-1}).[47]

Peptide stock solutions were 0.5 mM and heme stock solution was 5 mM. Heme-hIAPP complexes were prepared by incubating 1 equiv of hIAPP and 0.8 equiv of heme solutions for ∼6 h. Absorption spectra were recorded by adding 20 μL of the heme-IAPP complex solution in 1 mL of 100 mM pH 7 phosphate buffer. For the pH dependent absorption data, the peptide stock solution was added to 1 mL of 100 mM of the required buffer needed for the particular pH range. All the spectral data were obtained by an UV−vis diode array spectrophotometer (Agilent 8453).

The pH of the heme-hIAPP complexes for EPR spectra were calibrated to pH 7 using 1 M H_2SO_4. EPR spectra were obtained by a Jeol (JES FA200) spectrophotometer. 0.5 mM concentration samples were run at 77 K in a liquid nitrogen finger dewar flask.

Resonance Raman spectroscopy data were obtained at room temperature using a Trivista 555 spectrograph (Princeton Instruments) and 413.1 nm excitation from a Kr^+ laser (Coherent, Sabre Innova SBRC-DBW-K). Raman shifts were calibrated with naphthalene and indene. The wavenumber accuracy was ±1 cm^{-1} for well-defined peaks. The laser power was varied between 10 and 15 mW.

To obtain ferrous and ferrous-CO absorption spectra, all heme-hIAPP samples were degassed by purging with argon in anaerobic vials for ∼10 min. Absorption spectra were collected with heme-hIAPP samples (20 μL) in degassed 100 mM pH 7 phosphate buffer. Reduction of Fe^{3+} protein samples were carried out in anaerobic cuvettes by adding an anaerobically prepared stock solution of 20 mM sodium dithionite. CO adducts of heme(Fe^{2+})-hIAPP complexes were prepared by purging CO(g) through the headspace of septum-sealed cuvette with gentle agitation of the samples, until no further change was noticed in absorption spectra. CO(g) was generated by adding concentrated H_2SO_4 to ammonium formate and then passing the generated gas through 4 M KOH.

Cyclic Voltammetry (CV) was performed on a CH Instruments potentiostat (model CHI710D). An ingenious solution cell was prepared where a Teflon hollow disk was tightly fit on a graphite working electrode (∼100 μL volume). A Pt wire was used as the counter electrode, while an Ag wire was used as the reference electrode. Heme-hIAPP buffered solutions with 1 M KCl were prepared. The Fe^{3+}/Fe^{2+} potential for a 1 mM $K_4[Fe(CN)_6]$ solution in 1 M KCl was determined to be 200 mV using this setup, whose actual value is +450 mV versus NHE. Thus, the *E*-values measured against this Ag reference electrode were corrected by +250 mV to scale them versus NHE. The experiments were performed with degassed buffers in a glovebox to eliminate the O_2 reduction by the heme-hIAPP complex as well as from the graphite working electrode. Scan rate of 1 V/s was used to obtain the Fe^{3+}/Fe^{2+} potential. Heme CVs have been obtained at a high pH (pH ∼ 8−13) which is higher than the pK_a of the heme site (vide infra) and is thus the pure and physiologically relevant form.

3,3′,5,5′-Tetramethylbenzidine (TMB) was used as the substrate for peroxidase activity measurement. Ten milligrams of TMB was dissolved in 0.5 mL of glacial AcOH and 10 mL of AcOH/NaOAc buffer (1 M, pH 4.5). The solution was diluted to 25 mL with nanopure water and 100 μL, 30% H_2O_2 was added, followed by 10 μL of 0.05 mM of the protein sample. Kinetic traces were obtained by monitoring the increase of the 652 nm absorption band.

Catalase activity was measured by following the rate of decay of H_2O_2 at 240 nm. 1.5 mL of deionized water and 100 μL of 0.05 M H_2O_2 were mixed in a cuvette. Twenty microliters of 0.5 mM heme-hIAPP was added to it. All spectra were recorded in a kinetic mode, with continuous stirring at 25 °C.

For PROS calculation, the following xylenol orange assay was applied. A total of 4.9 mg of Mohr's salt and 3.9 mg of xylenol orange were dissolved in 5 mL of 250 mM H_2SO_4 and stirred for 10 min. A 200 μL portion of this solution was taken in 1.8 mL of nanopure water,

dx.doi.org/10.1021/ic4001413 | Inorg. Chem. 2013, 52, 5226−5235

Scheme 1. Amino Acid Sequence of (A) Human IAPP(1-37) Showing the Non-Amyloidogenic, Hydrophilic Region in Blue and the Hydrophobic Region in Yellow, Highlighting the Amyloidogenic Segment in Pink, (B) Human IAPP(1-19) Highlighting the Residues That Have Been Mutated in This Study; (C) Amino Acid Sequence of Human IAPP(1-22) without Disulfide Linkage; (D) Rat- IAPP(1-37) Highlighting the Sequence Differences with Human IAPP(1-37) in Green

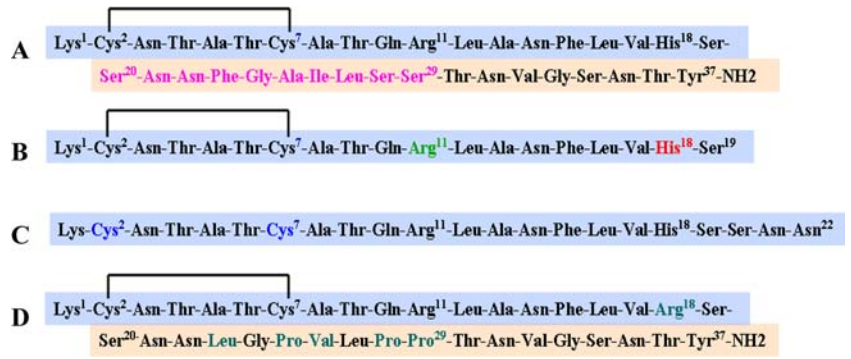

and a calibration curve for the quantitative estimation of H_2O_2 was obtained for 0.05, 0.1, 0.5, 1, 2.5, 5, and 10 μM concentrations of H_2O_2 by recording their absorbance at 560 nm. The calibration curve was expressed as absorbance at a fixed wavelength of 560 nm versus concentration of H_2O_2 in micromolar units for a 2 mL volume.[48] For the detection of PROS of the heme-hIAPP complex, a blank was obtained in the UV−vis spectrophotometer with 1.8 mL nanopure water in a cuvette. A total of 50 μL of 0.5 mM heme-hIAPP complex and 200 μL xylenol orange solution was added to the above cuvette and absorbance was measured. This served as the control. The heme-hIAPP complex was reduced using a minimal amount of dithionite under anaerobic conditions, followed by their reoxidation by O_2 (monitored by absorption). A total of 200 μL of 0.025 mM reoxidized solution was added to the cuvette containing the control, and absorbance of this solution was recorded. The value of absorbance of the above solution (after deducting the control) at 560 nm when plotted on the calibration curve yielded the corresponding H_2O_2 concentration.

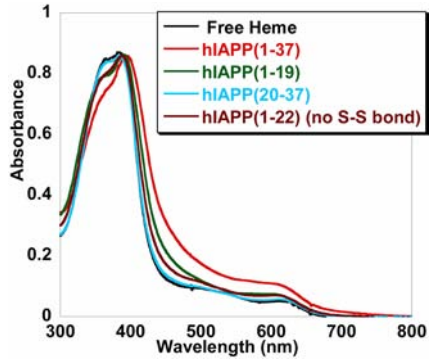

Figure 1. Absorption spectra of heme incubated hIAPP at pH 7: hIAPP(1−37), red; hIAPP(1−19), green; hIAPP(20−37), blue; hIAPP(1−22) (peptide without the disulfide linkage between Cys2 and Cys7), brown and free heme, black.

3. RESULTS AND ANALYSIS

3.1. Choice of Peptides. The human islet amyloid polypeptide (hIAPP) has 37 amino-acid residues. Two fragments, the hydrophilic hIAPP(1−19) and the amyloidogenic hIAPP(20−37) have been separately considered to identify the heme binding domain (Scheme 1A). There are three residues in hIAPP(1−19) that are known to bind heme biologically. There is one histidine, His18 (His binds heme in hemoglobin, myoglobin, cytochrome *c* oxidase, etc.) and two cysteine residues, Cys2 and Cys7 (Cys binds heme in cytochrome P450, nitric oxide synthase, etc.) (Scheme 1B). However, Cys2 and Cys7 are linked by a disulfide bridge, and hence the thiolate group of the cysteine residue will likely not be available for heme coordination (vide infra). There is a tyrosine residue, Tyr37, present in the amyloidogenic fragment (Scheme 1A), also known to bind heme biologically in catalases. To identify the heme binding residue, the following site directed mutants of hIAPP(1−19) were considered: single mutants His18Gly and His18Asn (Scheme 1B) to test the possibility of histidine coordination, single mutant Arg11Asn, double mutant Arg11Asn; His18Asn to understand the effects of both Arg11 and His18 (Scheme 1B), and the peptide fragment hIAPP(1−22) without the disulfide bridge (Scheme 1C).

3.2. Absorption Spectroscopy. The absorption spectra of 1 equiv of heme incubated with 1 equiv of hIAPP(1−37) and the isolated peptide fragments hIAPP(1−19) and hIAPP(20−37) overlaid with free heme are presented in Figure 1. There is an intensity decrease of the Soret band at ∼365 nm and a red shift of the 385 nm band to 398 nm in hIAPP(1−37). Further, the Q-band blue shifts from 618 to 605 nm with the development of a new band at 693 nm relative to that of free heme, indicating the formation of heme bound hIAPP(1−37) complex (Figure 1, red). The peptide fragment hIAPP(1−19) also shows similar spectral changes on incubating with heme, though the Soret band shifts from 385 to 392 nm, (Figure 1, green), thereby implicating that heme also binds to hIAPP(1−19).[49] However, heme does not bind to the peptide hIAPP(20−37) as the heme incubated spectrum looks identical to that of free heme (Figure 1, blue) even after prolonged incubation. This implies that the heme binding residue lies in the 1−19 fragment of the peptide sequence. This eliminates Tyr37 as the possible heme binding residue.

The peptide hIAPP(1−22), without the disulfide bridge between Cys2 and Cys7 also shows similar spectral changes relative to native hIAPP(1−19) (Figure 1, brown). Since the native peptide-heme complex and the heme complex of the variant without the disulfide bridge (this variant has the thiolate groups of Cys available for heme coordination) has similar spectral features, it possibly indicates that heme does not coordinate to the cysteine residues.

Thus, there exists only His18 available to coordinate to heme. Two single mutants His18Asn and His18Gly were each incubated with 1 equiv of heme. Incidentally, the absorption spectra of both mutants show the same characteristic features of

dx.doi.org/10.1021/ic4001413 | Inorg. Chem. 2013, 52, 5226−5235

the heme bound forms (Figure 2, orange and blue). Arginine residues in close vicinity of the active site are known to play key

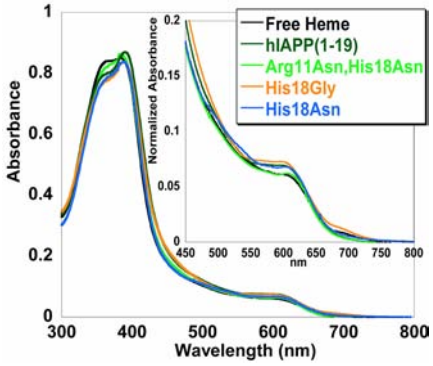

Figure 2. Absorption spectra of heme incubated hIAPP(1−19), green, and its mutants at pH 7: double mutant, Arg11Asn;His18Asn, bright green; histidine mutants, His18Gly, orange; His18Asn, blue; and free heme, black.

roles in heme based metalloenzymes or metallopeptide complexes.[50,51] Recent report in aldoxime dehydratase enzyme (OxdA) also observed that Arg178 residue is an important residue to anchor heme and heme content in the protein is low in the absence of Arg178.[46] There exists an arginine residue (Arg11) in the hIAPP(1−19) fragment. To probe any possible interaction of the arginine residue, a double mutant Arg11Asn; His18Asn was selected and incubated with heme. Interestingly, this mutant on incubating with heme shows spectral features identical to that of free heme, indicating that it does not bind heme (Figure 2, bright green). Thus from the absorption data we infer that heme possibly binds to His18 only in the presence of Arg11. Note that Arg11Asn mutant when incubated with heme also binds heme (Supporting Information, Figure S1). The fact that heme binds to hIAPP even in the absence of His18 (His18Asn mutant) possibly indicates additional interactions of the peptide with the heme cofactor (vide infra).

3.3. EPR Spectroscopy. Figure 3 shows the 77 K, X band EPR spectra of the heme-hIAPP(1−37) and heme-hIAPP(1−

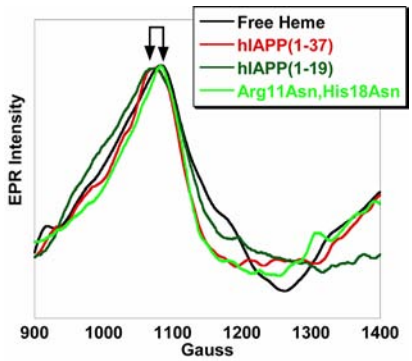

Figure 3. EPR spectra of free heme, black and heme-hIAPP complexes at pH 7: hIAPP(1−37), red; hIAPP(1−19), green; and double mutant Arg11Asn,His18Asn, bright green in the high field regions at 77 K.

19) complexes overlaid with free heme. The EPR spectra of the heme bound peptides are shifted to lower field relative to heme, indicating the formation of heme-bound species. The spectrum of the heme-peptide complexes shows an axial high spin ($S = 5/2$) Fe signal with $g \sim 6.0$ with the presence of small rhombic splitting. No high field, low spin signals were observed at this temperature. Thus hIAPP peptides bind heme to form an axial high-spin Fe^{3+} active site with rhombic distortion, similar to those found in myoglobin, hemoglobin, and several peroxidases.[52,53] Note that the EPR spectrum of the double mutant Arg11Asn,His18Asn is identical to that of free heme (Figure 3, bright green), further indicating that both His18 and Arg11 are essential for heme binding, consistent with the absorption data (Figure 2).

3.4. Resonance Raman Spectroscopy. The resonance Raman (rR) spectra in the high frequency region of the heme incubated hIAPP(1−37) and hIAPP(1−19) are overlaid with that of free heme in Figure 4. The oxidation state marker band,

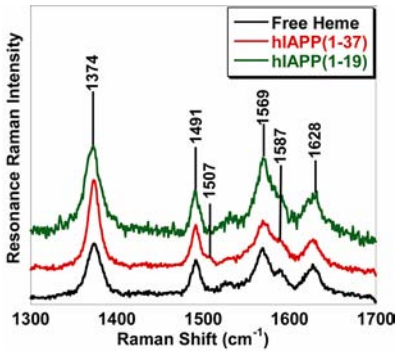

Figure 4. High frequency rR spectra of free heme, black, and heme-hIAPP complexes: hIAPP(1−37), red, and hIAPP(1−19), green, at pH 7 at room temperature.

ν_4, appears at 1374 cm^{-1}, as expected in ferric heme.[54] The vibrational frequencies sensitive to the core size of the heme macromolecule are ν_{10}, ν_3, and ν_2 and serve as the coordination number and spin state marker bands.[55] The ν_3 and ν_2 bands of both heme-hIAPP(1−37) and heme-hIAPP(1−19) complexes are observed at 1569 and 1491 cm^{-1}, respectively, (Figure 4, red and green respectively), while ν_{10}, the depolarized spin state marker band arises at 1628 cm^{-1} indicating a hexa-coordinated high spin ferric species with an exchangeable weak field distal ligand (such as H_2O) as observed in chloroperoxidase, cytochrome c peroxidase, horse radish peroxidase (HRP), and so forth.[56,57] There are present small intensities at 1587 (ν_2) and 1507 (ν_3) cm^{-1} in the rR data of hIAPP(1−37), indicative of formation of a relatively minor fraction of a six-coordinated low spin ferric species, which is absent in free heme (Figure 4, black).

3.5. Characterization of CO Binding to Ferrous Heme-hIAPP Complexes. Exogenous ligands like carbon monoxide (CO) can bind to the heme Fe from the distal site of the heme-hIAPP complexes. CO is an extremely useful probe for heme active sites.[58] Studies on CO adducts of heme proteins have been used to gain structural information, probe identity of the proximal ligands, and identify interactions between distal residues and CO, thereby providing insight into the nature of the heme environment.[59] The CO binding to heme-hIAPP complexes, their mutants, and free heme was tested by following their absorption spectra under anaerobic condition.

The absorption spectra of CO bound heme(Fe^{2+}) complexes of hIAPP(1−37), nonamyloidogenic segment hIAPP(1−19), and amyloidogenic fragment hIAPP(20−37) are overlaid with free heme(Fe^{2+})-CO in Figure 5. Binding of CO to reduced heme complexes of hIAPP(1−37) (Figure 5A and 5B, red) and

dx.doi.org/10.1021/ic4001413 | Inorg. Chem. 2013, 52, 5226−5235

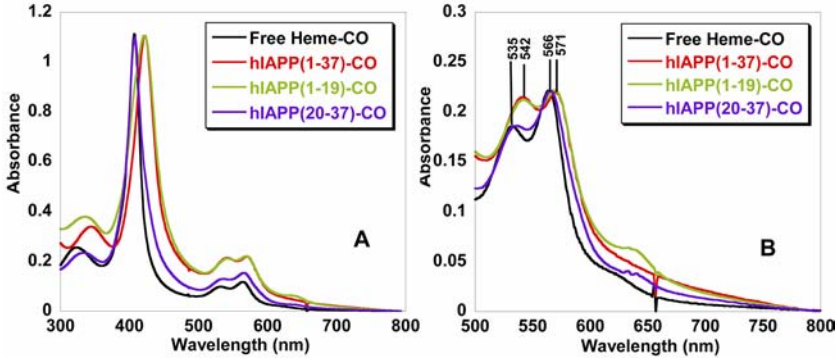

Figure 5. Absorption spectra of CO bound form of heme(Fe^{2+}) complexes of hIAPP at pH 7: (A) hIAPP(1−37),red; hIAPP(1−19), green; hIAPP(20−37), violet; and free heme, black. (B) Enlarged Q-band regions with assigned α and β bands.

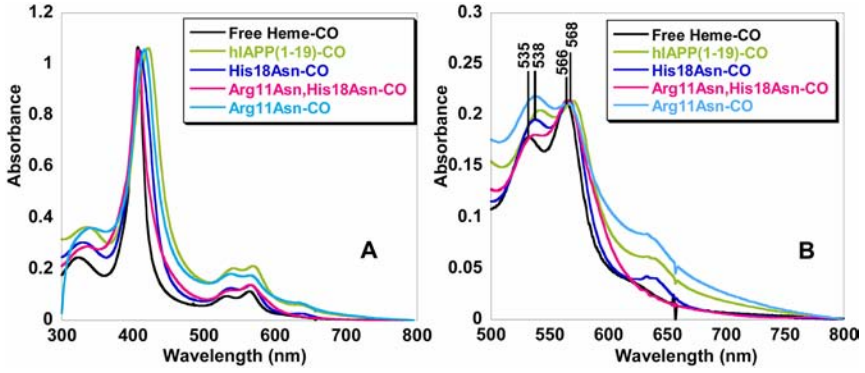

Figure 6. Absorption spectra of CO bound form of heme(Fe^{2+})-hIAPP complexes at pH 7: hIAPP(1−19), green; histidine mutant His18Asn, blue; double mutant Arg11Asn;His18Asn, pink; arginine mutant Arg11Asn, cyan; and free heme, black. (B) Enlarged Q-band regions with assigned α and β bands.

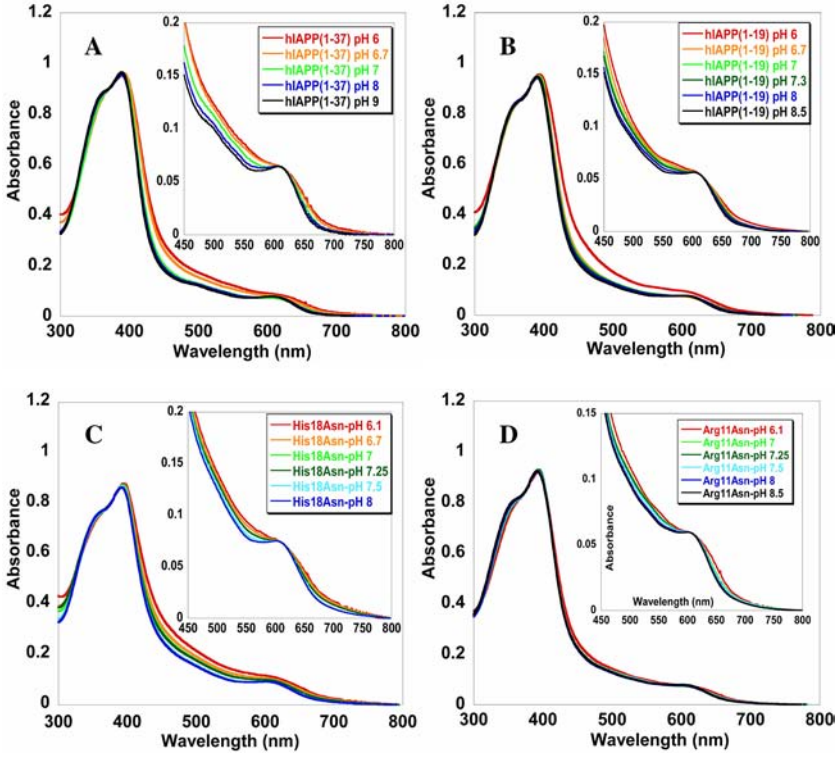

Figure 7. Absorption spectra of heme-hIAPP complexes at different pHs: (A) hIAPP(1−37), (B) hIAPP(1−19), (C) His18Asn mutant, and (D) Arg11Asn mutant. Inset: enlarged Q-band region.

dx.doi.org/10.1021/ic4001413 | *Inorg. Chem.* 2013, 52, 5226−5235

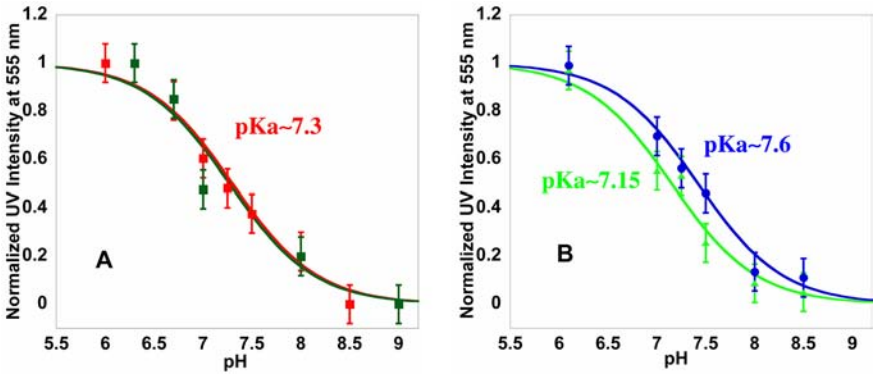

Figure 8. pK_a plots of heme-hIAPP complexes of (A) (1−37), red; (1−19), green; and (B) His18Asn mutant of (1−19), green, and Arg11Asn mutant, blue, with error bars. Six data points from Figure 7 have been used for each pK_a determination.

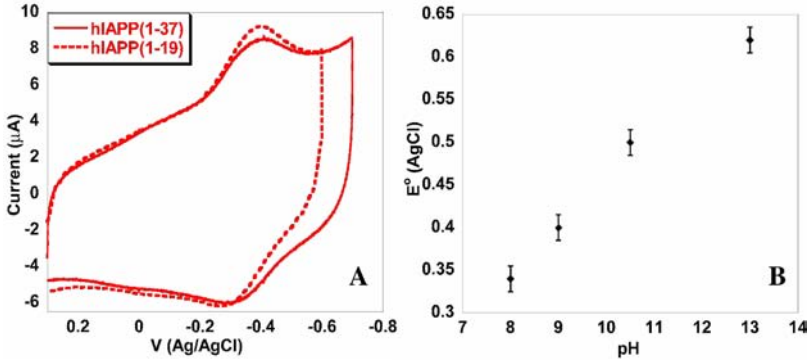

Figure 9. (A) Anaerobic CV at 1 V/s of heme-hIAPP(1−37) (red solid line) and hemehIAPP(1−19) (red dotted line) at pH 8. (B) $E°$ (vs AgCl) plot with the increase of pH of heme-hIAPP(1−37), black, with error bars.

hIAPP(1−19) (Figure 5A and 5B, green) results in the Soret maxima at 423 nm and α and β bands at 571 and 542 nm, respectively, consistent with a hexacoordinate heme active site with histidine residue as an axial ligand.[60−62] Similar spectroscopic features of the CO complex of heme(Fe^{2+})-hIAPP(1−22) (peptide without the disulfide linkage) are also observed (Supporting Information, Figure S1). This indicates that heme binding to hIAPP does not alter even in the absence of the disulfide bridge, consistent with the absorption data (Figure 1, brown). CO binding to reduced heme incubated complex of hIAPP(20−37) (Figure 5A and 5B, violet) results in a Soret maximum at 408 nm and α and β bands at 566 and 535 nm, respectively, identical to the CO bound spectra of free heme(Fe^{2+}) (Figure 5A and 5B, black). This further supports that heme does not bind to Tyr37 present in the hIAPP(20−37) peptide fragment, consistent with our above results (Figure 1, blue).

CO binding to heme(Fe^{2+}) complex of His18Asn mutant results in a Soret maximum at 410 nm and α and β bands at 568 and 538 nm, respectively (Figure 6A and 6B, blue). This is drastically different from the spectrum of the CO complex of native heme(Fe^{2+})-hIAPP(1−37) and heme(Fe^{2+})-hIAPP(1−19) (Figure 6A and 6B, green). This again indicates that probably His18 is the heme coordinating residue. The absorption spectrum of CO bound heme(Fe^{2+})-Arg11Asn mutant results in a Soret maximum at 418 nm and α and β bands at 566 and 538 nm, respectively (Figure 6A and 6B, cyan), which is also different than that of the wild type CO. This is in accordance to our inference that Arg11 residue strongly interacts with the active site. CO binding to the double mutant Arg11Asn;His18Asn results in the Soret maximum at 408 nm and α and β bands at 566 and 535 nm (Figure 6A and 6B, pink), respectively, identical to that of free heme(Fe^{2+})-CO (Figure 6A and 6B, black). Thus it further supports the fact that though heme binds to hIAPP peptides through the His18 residue, Arg11 residue is key for heme binding to hIAPP as indicated by the absorption data of the double mutant Arg11Asn;His18Asn (Figure 2, green) and its CO complex (Figure 6A and 6B, pink).

3.6. pH Perturbation and Trans Axial Ligand. Since the heme-hIAPP complexes bind exogenous ligands like CO, it likely implies the presence of a sixth exchangeable ligand trans to the axial His18 residue. The nature of the sixth ligand was investigated by pH perturbations. The heme-hIAPP(1−37) and hIAPP(1−19) complexes exhibit an increase in the Soret band (∼ 365 nm) and a decrease in the Q-band (∼ 635 nm) intensities and a blue shift of the Q-band on going from low to high pH (Figure 7A and 7B) with a pK_a of ∼7.3 ± 0.2 (Figure 8, red and green). Similar spectral changes with changes in pH are observed for the His18Asn mutant (Figure 7C), but the pK_a obtained was ∼7.15 ± 0.2 (Figure 8, orange), lower than that in native hIAPP peptides. The pK_a of Arg11Asn mutant was ∼7.6 ± 0.2 (Figure 7D) which is slightly higher than the wild type hIAPP. The observed pK_a of ∼7.3 likely indicates the presence of a water derived ligand.[33,56] This is also confirmed by the rR data (Figure 4).

3.7. Cyclic Voltammetry. Cyclic Voltammerty (CV) of native heme-hIAPP complexes shows reversible process under anaerobic condition (Figure 9). Free heme has a reduction potential of 0.20 V vs NHE.[63] The heme-hIAPP(1−37) shows

dx.doi.org/10.1021/ic4001413 | Inorg. Chem. 2013, 52, 5226−5235

a Fe^{3+}/Fe^{2+} redox process at −0.36 V (Figure 9A, red solid line), while heme-hIAPP(1−19) show a Fe^{3+}/Fe^{2+} redox process at −0.34 V (Figure 9A, red dotted line) at pH 8. The redox potential changes by ∼0.056 V per unit change in pH in the pH range of 8−13 for heme-hIAPP(1−37) (Figure 9B). This indicates that the reduction of Fe^{3+} to Fe^{2+} involves a proton coupled electron transfer (PCET) process involving one proton.[64−66] This is consistent with a $Fe^{3+}(H_2O) \rightarrow Fe^{2+}(HO^-)$ redox process at the active site.

3.8. Reactivity. *3.8.1. Peroxidase Activity.* Peroxidases are heme based metalloenzymes with a coordinated histidine residue containing a conserved arginine residue in the distal pocket that provides protons for the O−O bond cleavage of H_2O_2 in the catalytic cycle.[50,67] The peroxidase activity of the native heme-hIAPP complexes and free heme were tested by following the catalytic oxidation of substrate, 3,3′,5,5′-tetramethylbenzidine (TMB), by H_2O_2. The heme-hIAPP(1−37) and heme-hIAPP(1−19) do not show any enhanced peroxidase activity relative to that of free heme (Figure 10). The Arg11 mutant also did not exhibit any peroxidase activity relative to free heme (Supporting Information, Figure S3).

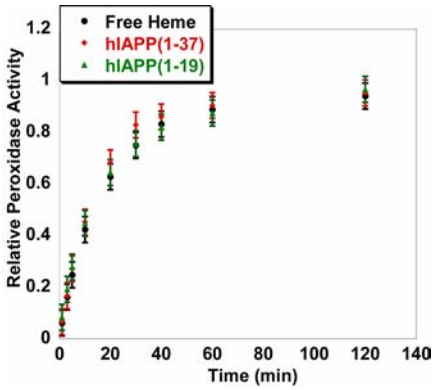

Figure 10. Kinetic traces for relative peroxidase activity, monitoring the increase of the 652 nm absorbance intensity, for the native heme-hIAPP complexes: hIAPP(1−37), red; hIAPP(1−19), green; and free heme, black.

3.8.2. Catalase Activity. The catalase (tyrosine coordinated heme enzyme) activity of the heme-hIAPP complexes show that these heme complexes do not show any catalase activity with respect to free heme (Supporting Information, Figure S4). This indicates that Tyr37 does not coordinate to heme to form any catalase type active sites.[68] This further supports the conclusion drawn from spectroscopy that the heme binding domain lies in the peptide segment IAPP(1−19).

3.8.3. PROS Generation. The reduction of O_2 by heme-(Fe^{2+})-hIAPP complexes was investigated under homogeneous condition. When 1 equiv of dithionite was added to the heme-hIAPP peptide solutions, the resting Fe^{3+} site of heme was reduced to Fe^{2+} (Supporting Information, Figure S5). When O_2 was introduced to the either fully reduced heme(Fe^{2+})-hIAPP(1−37) or heme(Fe^{2+})-hIAPP(1−19) complexes, it reoxidized the Fe^{2+} to the Fe^{3+} form as indicated by absorption spectroscopy (Supporting Information, Figure S5A and S5B). In this process the O_2 gets reduced. This reduction of O_2 by the heme(Fe^{2+})-hIAPP peptides can either produce superoxide $(O_2^{\bullet-})$, H_2O_2, or it could be a 4 e^-/4 H^+ process leading to the formation of H_2O. Any H_2O_2 formed during the O_2 reduction process (either due to the 2 e^- reduction of O_2 or by the disproportionation of $O_2^{\bullet-}$) has been detected by using the xylenol orange assay (Materials and Methods Section). The results indicate that heme(Fe^{2+})-hIAPP(1−37) produces 40 ± 5% H_2O_2 and heme(Fe^{2+})-hIAPP(1−19) generates 38 ± 5% H_2O_2.

4. DISCUSSION

The results presented in this study indicate that the hIAPP peptides associated with T2Dm bind heme, and the heme binding domain resides in the nonamyloidogenic 1−19 segment of hIAPP. From the EPR and rR data it is evident that heme-hIAPP complexes form an axial high spin Fe^{3+} active site with an $S = 5/2$ ground state. There exist three heme coordinating residues in the hydrophilic peptide fragment hIAPP(1−19), His18, Cys2, and Cys7, that are known to bind heme biologically. There is also a Tyr37 residue present in the amyloidogenic peptide fragment IAPP(20−37) that can possibly bind heme. Since the peptide fragment IAPP(20−37) does not bind heme, even after prolonged incubation (Figure 1, blue), Tyr37 is not the heme coordinating residue. This is further supported by the lack of catalase activity of these heme-IAPP complexes (Supporting Information, Figure S4), implying that no tyrosine coordinated catalase type active site results on heme binding to hIAPP peptides. Cys2 and Cys7 are linked by a disulfide bond due to which the thiolate side chain of cysteine is not available for heme binding to the peptides. When heme was incubated with hIAPP(1−22), peptide without the disulfide bond between Cys2 and Cys7, the resultant absorption spectrum (Figure 1, brown) was identical to that of the heme bound hIAPP(1−37) and hIAPP(1−19) complexes, implying that cysteine probably does not coordinate to heme bound hIAPP. This conclusion is further substantiated when the CO complex of heme(Fe^{2+})-hIAPP(1−22) (peptide without disulfide linkage) showed similar spectral features (Supporting Information, Figure S2) to that of CO complex of heme(Fe^{2+})-hIAPP(1−19) (Figure 5, green). Thus, His18 is the only other residue available to coordinate heme. The CO complex of heme(Fe^{2+})-hIAPP has the Soret band at 423 nm and α and β bands at 571 and 542 nm respectively, indicating a histidine ligated six coordinate heme active site.[61,62,69] Interestingly, the absence of His18 (His18Asn and His18Gly mutants, Figure 2) also indicates heme binding to the peptide. However, the double mutant Arg11Asn;His18Asn does not bind heme (Figure 2, bright green), reflecting that though His18 is the heme coordinating residue, Arg11 plays a crucial role in heme binding and Arg11 binds heme in the His18 mutants. This is further reflected by the absorption data of the CO complex of the His18Asn mutant, which shows a shift in the Soret band from 423 nm in the native hIAPP peptide to 410 nm in the mutant (Figure 6A and 6B, blue), indicating that His18 is likely involved in heme binding. The CO complex of the Arg11Asn mutant has the Soret maximum at 418 nm (Figure 6A and 6B, cyan), relative to 423 nm in the native hIAPP, further implicating that Arg11 is also involved in heme binding. Further, the absorption data of the CO complex of His18Asn;Arg11Asn double mutant is identical to that of free heme (Figure 6A and 6B, pink), indicating that both His18 and Arg11 are essential for heme binding to hIAPP peptides.

Arginine residues are known to act as key second sphere residues in heme based metalloproteins and peptides, providing protons for catalytic reactions.[33,50] The Arg11 residue can interact with heme in any of the following three ways: (i) bind heme as an axial ligand along with His18, (ii) hydrogen bond

dx.doi.org/10.1021/ic4001413 | Inorg. Chem. 2013, 52, 5226−5235

with either the proximal His18 residue or the distal water derived ligand, and (iii) hydrogen bond or ion pair (arginine is positively charged and the heme propionate groups are negatively charged at pH 7) with the propionate side chains of heme. The first possibility is unlikely as there are no reported cases of Arg binding to heme in biological systems, although Arg is known to bind to the nonheme Fe active site of Biotin Synthase.[70,71] Furthermore, a six coordinate Fe^{3+} active site with six nitrogen donor ligands is almost certain to be low spin and not high spin as observed for this active site (Figure 3 and 4). The second possibility where Arg11 hydrogen bonds with the NH of His18 (which is a hydrogen bond donor) is unlikely as the lone pair of Arg11 will be protonated at pH 7, that is, it can not accept a hydrogen bond. Hydrogen bonding to the distal water derived ligand is quite likely. But this does not explain the binding of heme to hIAPP even in the absence of His18 (i.e., His18Asn and His18Gly mutants) and the relatively small shift in pK_a of the trans axial H_2O ligand upon mutation of the Arg11 residue. The third possibility, where Arg11 hydrogen bonds with the propionate side chain of heme along with His18 coordination to heme, allows heme binding to both His18Asn and His18Gly mutants (via Arg11 hydrogen bonding or ion pairing with the propionate side chains of heme) and Arg11Asn mutant (heme binding via His18). This has been observed in the active site soluble Guanylate Cyclase (sGC), where it has been shown that protoporphyrin IX (heme without the Fe) can bind to the active site and be held tightly in position by hydrogen bonding interactions between the propionate side chain of heme and Arg139.[72] Similarly, on binding NO to sGC, the proximal histidine ligand (His105) dissociates from the active side, while the heme is held by hydrogen bonding interactions with Arg139. If the Arg11 group is held near the propionate side chains of the heme, the distance of the Arg11 from the active site would prevent it from exerting the pull effect required for exhibiting peroxidase activity (Figure 10). Similarly the lack of direct hydrogen bonding interaction with the distal water ligand would lead to a negligible shift of pK_a for the Arg11 mutant (Figure 7D and 8B) relative to the wild type.

CV data at around physiological pH indicate that the heme sites (E° = −0.34 V, i.e., −0.11 vs NHE) can be reduced by physiological reducing agents like glutathione (E° = −0.25 V vs NHE)[73] and NADH (E° = −0.45 V vs NHE).[74] The reduced heme-IAPP complexes when exposed to O_2 generate H_2O_2 which has been quantified. The 1 e^- reduction of O_2 produces superoxide, $O_2^{\bullet-}$, which after disproportionation should yield ∼50% H_2O_2. The 2 e^- reduction of O_2 on the other hand produces 100% H_2O_2. Experimentally ∼40% PROS has been estimated for the heme-hIAPP complexes indicating that only 1 e^- is being donated by the reduced metal center to O_2 in aqueous buffered solutions having physiological pH.

The pancreatic β-cells are extraordinarily sensitive to damage from PROS generation compared to other cells found in skeletal muscles, liver, kidney, brain, and so forth.[17,75] Thus heme binding to hIAPP(1−37) and the PROS generation from oxidation of the reduced heme-hIAPP(1−37) complex by molecular O_2 provide a vital explanation for the extreme susceptibility of pancreatic β-cells toward oxidative stress and the reduction of β-cell mass and its dysfunction in T2Dm. Compromised mitochondrial activity and its reduced content, heightened oxidative stress which consequently leads to altered insulin sensitivity have been proposed to be an underlying feature of obesity-driven T2Dm.[76] The disruption of mitochondrial structure and function leads to profound effect on mitochondrial iron concentration and heme homeostasis, decreasing the activity of iron-containing enzymes and complexes of the electron transport chain (ETC), which gives rise to more fatty acid oxidation and increased risk of developing T2Dm.[77] Recent studies have shown that IAPP deposits not only are exclusive in pancreatic islets but also are found in kidneys,[78] heart,[79] with higher plasma concentration in T2Dm patients than in controls. Hyperamylinemia have been shown to induce risks like diabetic nephropathy and hampered renal functions, altered cardiac myocyte structure and function that contribute to progressive heart failure.[78,79] Thus disrupted heme homeostasis, compromised mitochondrial metabolism, deposits of IAPP in organs like kidney, heart besides pancreatic islets, along with our finding of heme binding to hIAPP under physiological conditions and the associated PROS generation provide an insight that heme may play a greater role in T2Dm than previously comprehended.

Both AD and T2Dm have been demonstrated to share common modes of toxic pathway through mitochondrial dysfunction.[39] Specifically, in both the diseases there occurs significant reduction in complex IV activity, mitochondrial respiration and increased PROS formation.[39,80] Heme binding to Aβ peptide associated with AD followed by subsequent aberrations in the heme biogenesis pathway have been linked to mitochondrial decay in AD.[34,81] Similar epidemiological features between AD and T2Dm suggest that heme binding to hIAPP might be responsible for the loss of β-cells in T2Dm. His13 residue in Aβ peptides binds heme under physiological conditions and results in an axial high-spin active site with a trans-axial water derived ligand, while acidic Agr5 residue present at the distal side is responsible for the peroxidase activity of these complexes.[33] The active site environment of heme-hIAPP is similar to that of heme-Aβ, as His18 binds heme with a trans-axial water derived ligand. However, Arg11 possibly directly hydrogen bonds with the propionate side chains of heme, thereby it is also essential for heme binding. However, the heme-hIAPP complexes do not function as peroxidase like heme-Aβ complexes, suggesting that the Arg11 is not available in the distal pocket to provide any proton required to drive O−O bond heterolysis.

The hallmark of both AD and T2Dm is heightened oxidative stress and PROS formation.[38] While heme(Fe^{2+})-Aβ reduces O_2 by 2 e^- to H_2O_2 quantitatively,[48] heme(Fe^{2+})-hIAPP produces ∼40% H_2O_2 through 1 e^- reduction of O_2. This is because the Tyr10 residue of Aβ peptides is redox active and donates an electron to O_2 along with the reduced heme center leading to a 2 e^- reduction of O_2 to H_2O_2. On the contrary, the Tyr37 residue in hIAPP is not involved in O_2 reduction by reduced heme-hIAPP complex which can, therefore, reduce O_2 only by 1 e^- to O_2^-. This is likely due to the close proximity of the Tyr10 residue to the heme coordinating His13 residue in heme-Aβ peptides. In the case of heme-hIAPP the heme coordinating residue His18 is possibly not in the vicinity of the Tyr37 residue.

It is important to note that rats are not affected by T2Dm. Rat-IAPP is nonamyloidogenic and differs from hIAPP at 6 amino acid residues (Scheme 1D). Five sequence differences mainly reside in the 20−29 peptide domain and are known to reduce its amyloidogenicity, while the major change is the replacement of His18 by an Arg in the nonamyloidogenic part.[10,82] The fact that the His18 residue involved in heme binding to hIAPP is absent in rat-IAPP is very interesting and

dx.doi.org/10.1021/ic4001413 | Inorg. Chem. 2013, 52, 5226−5235

stresses the possible importance of heme binding to hIAPP in the pathology of T2Dm.

5. CONCLUSION

In conclusion, we have established that heme binds to human IAPP. The heme binding domain lies in the 1−19 non-amylodogenic segment of hIAPP. His18 of hIAPP peptides binds heme at the proximal site. The open distal side of the heme-hIAPP complex has an exchangeable water derived ligand with a pK_a 7.3. The Arg11 is a key residue that directly hydrogen bonds with the propionate side chain of heme and plays an important role in heme binding to hIAPP. These findings illustrate the nature of the interaction of heme with hIAPP peptides which is fundamental in unraveling the role played by heme in T2Dm. Heme(Fe^{2+})-hIAPP complexes reduce O_2 by 1 e^- to produce ∼40% H_2O_2. The electrochemical data around physiological pH suggests that heme-hIAPP complexes can be reduced by physiological reductants and are prone to generate cytotoxic PROS and oxidative stress. The His18 residue of hIAPP, involved in heme binding, is absent in rat IAPP. Incidentally, rats do not get affected by T2Dm, further implying the importance of heme in the onset and development of T2Dm.

■ ASSOCIATED CONTENT

Supporting Information

Absorption spectrum of Arg11Asn mutant, CO bound heme-hIAPP(1−22) complex, peroxidase activity of Arg11Asn mutant, catalase activity plot of heme-hIAPP complexes, and the 1 equivalent reduction by dithionite and consequent reoxidation by O_2 of heme-hIAPP complexes. This material is available free of charge via the Internet at http://pubs.acs.org.

■ AUTHOR INFORMATION

Corresponding Author

*E-mail: icsgd@iacs.res.in.

Notes

The authors declare no competing financial interest.

■ ACKNOWLEDGMENTS

We thank IACS for funding this research. S.M. is thankful to the Council of Scientific and Industrial Research, India, for a Junior Research Fellowship. We thank Dr. Abhishek Dey for helpful discussions along with use of the resonance Raman instrument (DST, India, Grant-SR/IC-35/2009) and Sudipta Chatterjee for help with CV experiments.

■ REFERENCES

(1) Höppener, J. W. M.; Ahrén, B.; Lips, C. J. M. *N. Engl. J. Med.* **2000**, *343*, 411.
(2) Hardy, J.; Selkoe, D. J. *Science* **2002**, *297*, 353.
(3) Chiti, F.; Dobson, C. M. *Annu. Rev. Biochem.* **2006**, *75*, 333.
(4) Lorenzo, A.; Razzaboni, B.; Weir, G. C.; Yankner, B. A. *Nature* **1994**, *368*, 756.
(5) Kahn, S. E.; Andrikopoulos, S.; Verchere, C. B. *Diabetes* **1999**, *48*, 241.
(6) Westermark, P.; Wernstedt, C.; Wilander, E.; Hayden, D. W.; O'Brien, T. D.; Johnson, K. H. *Proc. Natl. Acad. Sci. U.S.A.* **1987**, *84*, 3881.
(7) Cooper, G. J.; Willis, A. C.; Clark, A.; Turner, R. C.; Sim, R. B.; Reid, K. B. *Proc. Natl. Acad. Sci. U.S.A.* **1987**, *84*, 8628.
(8) Kahn, S. E.; D'Alessio, D. A.; Schwartz, M. W.; Fujimoto, W. Y.; Ensinck, J. W.; Taborsky, G. J.; Porte, D. *Diabetes* **1990**, *39*, 634.
(9) Leighton, B.; Cooper, G. J. S. *Nature* **1988**, *335*, 632.
(10) Madine, J.; Jack, E.; Stockley, P. G.; Radford, S. E.; Serpell, L. C.; Middleton, D. A. *J. Am. Soc. Chem.* **2008**, *130*, 14990.
(11) Mirzabekov, T. A.; Lin, M.-c.; Kagan, B. L. *J. Biol. Chem.* **1996**, *271*, 1988.
(12) Zhang, S.; Liu, J.; Dragunow, M.; Cooper, G. J. S. *J. Biol. Chem.* **2003**, *278*, 52810.
(13) Anguiano, M.; Nowak, R. J.; Lansbury, P. T. *Biochemistry* **2002**, *41*, 11338.
(14) Janson, J.; Ashley, R. H.; Harrison, D.; McIntyre, S.; Butler, P. C. *Diabetes* **1999**, *48*, 491.
(15) Lin, C.-Y.; Gurlo, T.; Kayed, R.; Butler, A. E.; Haataja, L.; Glabe, C. G.; Butler, P. C. *Diabetes* **2007**, *56*, 1324.
(16) Kayed, R.; Head, E.; Thompson, J. L.; McIntire, T. M.; Milton, S. C.; Cotman, C. W.; Glabe, C. G. *Science* **2003**, *300*, 486.
(17) Zraika, S.; Hull, R. L.; Udayasankar, J.; Aston-Mourney, K.; Subramanian, S. L.; Kisilevsky, R.; Szarek, W. A.; Kahn, S. E. *Diabetologia* **2009**, *52*, 626.
(18) Haataja, L.; Gurlo, T.; Huang, C. J.; Butler, P. C. *Endocr. Rev.* **2008**, *29*, 303.
(19) Masad, A.; Hayes, L.; Tabner, B. J.; Turnbull, S.; Cooper, L. J.; Fullwood, N. J.; German, M. J.; Kametani, F.; El-Agnaf, O. M. A.; Allsop, D. *FEBS Lett.* **2007**, *581*, 3489.
(20) Fernandez-Real, J. M.; Lopez-Bermejo, A.; Ricart, W. *Diabetes* **2002**, *51*, 2348.
(21) Swaminathan, S.; Fonseca, V. A.; Alam, M. G.; Shah, S. V. *Diabetes Care* **2007**, *30*, 1926.
(22) Rajpathak, S. N.; Crandall, J. P.; Wylie-Rosett, J.; Kabat, G. C.; Rohan, T. E.; Hu, F. B. *Biochim. Biophys. Acta* **2009**, *1790*, 671.
(23) Giugliano, D.; Ceriello, A.; Paolisso, G. *Diabetes Care* **1996**, *19*, 257.
(24) Cooksey, R. C.; Jouihan, H. A.; Ajioka, R. S.; Hazel, M. W.; Jones, D. L.; Kushner, J. P.; McClain, D. A. *Endocrinology* **2004**, *145*, 5305.
(25) Tiedge, M.; Lortz, S.; Drinkgern, J.; Lenzen, S. *Diabetes* **1997**, *46*, 1733.
(26) Wilson, J. G.; Lindquist, J. H.; Grambow, S. C.; Crook, E. D.; Maher, J. F. *Am. J. Med. Sci.* **2003**, 325.
(27) Ferrannini, E. *Lancet* **2000**, *355*, 2181.
(28) Green, A.; Basile, R.; Rumberger, J. M. *Metabolism* **2006**, *55*, 1042.
(29) Lenzen, S.; Drinkgern, J.; Tiedge, M. *Free Radical Biol. Med.* **1996**, *20*, 463.
(30) Rauk, A. *Chem. Soc. Rev.* **2009**, *38*, 2698.
(31) Masters, C. L.; Simms, G.; Weinman, N. A.; Multhaup, G.; McDonald, B. L.; Beyreuther, K. *Proc. Natl. Acad. Sci.* **1985**, *82*, 4245.
(32) Atamna, H.; Frey, W. H. *Proc. Natl. Acad. Sci.* **2004**, *101*, 11153.
(33) Pramanik, D.; Dey, S. G. *J. Am. Soc. Chem.* **2011**, *133*, 81.
(34) Pramanik, D.; Ghosh, C.; Mukherjee, S.; Dey, S. G. *Coord. Chem. Rev.* **2013**, *257*, 81.
(35) Kimpara, T.; Takeda, A.; Yamaguchi, T.; Arai, H.; Okita, N.; Takase, S.; Sasaki, H.; Itoyama, Y. *Neurobiol. Aging* **2000**, *21*, 551.
(36) Schipper, H. M.; Cissé, S.; Stopa, E. G. *Ann. Neurol.* **1995**, *37*, 758.
(37) Atamna, H.; Liu, J.; Ames, B. N. *J. Biol. Chem.* **2001**, *276*, 48410.
(38) Grűnblatt, E.; Bartl, J.; Riederer, P. *J. Neural Transm.* **2011**, *118*, 371.
(39) Lim, Y.-A.; Rhein, V.; Baysang, G.; Meier, F.; Poljak, A.; J. Raftery, M.; Guilhaus, M.; Ittner, L. M.; Eckert, A.; Götz, J. *Proteomics* **2010**, *10*, 1621.
(40) Rajpathak, S.; Ma, J.; Manson, J.; Willett, W. C.; Hu, F. B. *Diabetes Care* **2006**, *29*, 1370.
(41) Zhao, Z.; Li, S.; Liu, G.; Yan, F.; Ma, X.; Huang, Z.; Tian, H. *PLoS ONE* **2012**, *7*, e41641.
(42) Bao, W.; Rong, Y.; Rong, S.; Liu, L. *BMC Med.* **2012**, *10*, 119.
(43) Qiu, C.; Zhang, C.; Gelaye, B.; Enquobahrie, D. A.; Frederick, I. O.; Williams, M. A. *Diabetes Care* **2011**, *34*, 1564.
(44) Damm, P. *Dan. Med. Bull.* **1998**, *45*, 495.
(45) Mukerji, G.; Chiu, M.; Shah, B. R. *Diabetologia* **2012**, *55*, 2148.

(46) Nomura, J.; Hashimoto, H.; Ohta, T.; Hashimoto, Y.; Wada, K.; Naruta, Y.; Oinuma, K.-I.; Kobayashi, M. *Proc. Natl. Acad. Sci. U.S.A.* **2013**, *110*, 2810.
(47) Yi, L.; Ragsdale, S. W. *J. Biol. Chem.* **2007**, *282*, 21056.
(48) Pramanik, D.; Ghosh, C.; Dey, S. G. *J. Am. Soc. Chem.* **2011**, *133*, 15545.
(49) The absorption features of heme incubated hIAPP(1−37) were quite broader than that of hIAPP(1−19) due to some scattering of hIAPP(1−37) in 100 mM pH 7 phosphate buffer.
(50) Rodriguez-Lopez, J. N.; Smith, A. T.; Thorneley, R. N. F. *J. Biol. Chem.* **1996**, *271*, 4023.
(51) Qian, J.; Mills, D. A.; Geren, L.; Wang, K.; Hoganson, C. W.; Schmidt, B.; Hiser, C.; Babcock, G. T.; Durham, B.; Millett, F.; Ferguson-Miller, S. *Biochemistry* **2004**, *43*, 5748.
(52) Rotilio, G.; Calabrese, L.; Giacometti, G. M.; Brunori, M. *Biochim. Biophys. Acta* **1971**, *236*, 234.
(53) Peisach, J.; Blumberg, W. E.; Wittenberg, B. A.; Wittenberg, J. B.; Kampa, L. *Proc. Natl. Acad. Sci. U.S.A.* **1969**, *63*, 934.
(54) Spiro, T. G.; Burke, J. M. *J. Am. Soc. Chem.* **1976**, *98*, 5482.
(55) Callahan, P. M.; Babcock, G. T. *Biochemistry* **1981**, *20*, 952.
(56) Dasgupta, S.; Rousseau, D. L.; Anni, H.; Yonetani, T. *J. Biol. Chem.* **1989**, *264*, 654.
(57) Mukai, M.; Nagano, S.; Tanaka, M.; Ishimori, K.; Morishima, I.; Ogura, T.; Watanabe, Y.; Kitagawa, T. *J. Am. Soc. Chem.* **1997**, *119*, 1758.
(58) Ray, G. B.; Li, X. Y.; Ibers, J. A.; Sessler, J. L.; Spiro, T. G. *J. Am. Soc. Chem.* **1994**, *116*, 162.
(59) Frauenfelder, H.; Sligar, S. G.; Wolynes, P. G. *Science* **1991**, *254*, 1598.
(60) Blumberg, W. E.; Peisach, J.; Wittenberg, B. A.; Wittenberg, J. B. *J. Biol. Chem.* **1968**, *243*, 1854.
(61) Pond, A. E.; Roach, M. P.; Thomas, M. R.; Boxer, S. G.; Dawson, J. H. *Inorg. Chem.* **2000**, *39*, 6061.
(62) Peisach, J.; Blumberg, W. E.; Wittenberg, B. A.; Wittenberg, J. B. *J. Biol. Chem.* **1968**, *243*, 1871.
(63) Moffet, D. A.; Foley, J.; Hecht, M. H. *Biophys. Chem.* **2003**, *105*, 231.
(64) Hammes-Schiffer, S. *Acc. Chem. Res.* **2009**, *42*, 1881.
(65) Costentin, C.; Robert, M.; Savéant, J.-M. *Acc. Chem. Res.* **2010**, *43*, 1019.
(66) Mayer, J. M. *Acc. Chem. Res.* **2011**, *44*, 36.
(67) Henriksen, A.; Smith, A. T.; Gajhede, M. *J. Biol. Chem.* **1999**, *274*, 35005.
(68) Diaz, A.; Loewen, P. C.; Fita, I.; Carpena, X. *Arch. Biochem. Biophys.* **2012**, *525*, 102.
(69) Vogel, K. M.; Hu, S.; Spiro, T. G.; Dierks, E. A.; Yu, A. E.; Burstyn, J. N. *J. Biol. Inorg. Chem.* **1999**, *4*, 804.
(70) Jarrett, J. T. *Arch. Biochem. Biophys.* **2005**, *433*, 312.
(71) Berkovitch, F.; Nicolet, Y.; Wan, J. T.; Jarrett, J. T.; Drennan, C. L. *Science* **2004**, *303*, 76.
(72) Schmidt, P. M.; Schramm, M.; Schröder, H.; Wunder, F.; Stasch, J.-P. *J. Biol. Chem.* **2004**, *279*, 3025.
(73) Ãslund, F.; Berndt, K. D.; Holmgren, A. *J. Biol. Chem.* **1997**, *272*, 30780.
(74) Unden, G.; Bongaerts, J. *Biochim. Biophys. Acta* **1997**, *1320*, 217.
(75) Kahn, S. E. *Diabetologia* **2003**, *46*, 3.
(76) Kim, J.-Y.; van de Wall, E.; Laplante, M.; Azzara, A.; Trujillo, M. E.; Hofmann, S. M.; Schraw, T.; Durand, J. L.; Li, H.; Li, G.; Jelicks, L. A.; Mehler, M. F.; Hui, D. Y.; Deshaies, Y.; Shulman, G. I.; Schwartz, G. J.; Scherer, P. E. *J. Clin. Invest.* **2007**, *117*, 2621.
(77) Huang, J.; Jones, D.; Luo, B.; Sanderson, M.; Soto, J.; Abel, E. D.; Cooksey, R. C.; McClain, D. A. *Diabetes* **2011**, *60*, 80.
(78) Gong, W.; Liu, Z. H.; Zeng, C. H.; Peng, A.; Chen, H. P.; Zhou, H.; Li, L. S. *Kidney Int.* **2007**, *72*, 213.
(79) Despa, S.; Margulies, K. B.; Chen, L.; Knowlton, A. A.; Havel, P. J.; Taegtmeyer, H.; Bers, D. M.; Despa, F. *Circ. Res.* **2012**, *110*, 598.
(80) Green, K.; Brand, M. D.; Murphy, M. P. *Diabetes* **2004**, *53*, S110.
(81) Atamna, H.; Frey, Ii, W. H. *Mitochondrion* **2007**, *7*, 297.
(82) Goldsbury, C.; Goldie, K.; Pellaud, J.; Seelig, J.; Frey, P.; Muller, S. A.; Kistler, J.; Cooper, G. J. S.; Aebi, U. *J. Struct. Biol.* **2000**, *130*, 352.